analytical chemistry

pubs.acs.org/ac Article

Ultrasensitive and Simultaneous SERS Detection of Multiplex MicroRNA Using Fractal Gold Nanotags for Early Diagnosis and Prognosis of Hepatocellular Carcinoma

Jiamin Wu, Xia Zhou, Ping Li, Xiaoling Lin, Jinhua Wang, Ziwei Hu, Pengcheng Zhang, Dong Chen, Huaihong Cai, Reinhard Niessner, Christoph Haisch, Pinghua Sun,* Yun Zheng,* Zhengjin Jiang,* and Haibo Zhou*

Cite This: *Anal. Chem.* 2021, 93, 8799−8809 Read Online

ACCESS | Metrics & More | Article Recommendations | Supporting Information

ABSTRACT: Sensitive and simultaneous detection of multiple cancer-related biomarkers in serum is essential for diagnosis, therapy, prognosis, and staging of cancer. Herein, we proposed a magnetically assisted sandwich-type surface-enhanced Raman scattering (SERS)-based biosensor for ultrasensitive and multiplex detection of three hepatocellular carcinoma-related microRNA (miRNA) biomarkers. The biosensor consists of an SERS tag (probe DNA-conjugated DNA-engineered fractal gold nanoparticles, F-AuNPs) and a magnetic capture substrate (capture DNA-conjugated Ag-coated magnetic nanoparticles, AgMNPs). The proposed strategy achieved simultaneous and sensitive detection of three miRNAs (miRNA-122, miRNA-223, and miRNA-21), and the limits of detection of the three miRNAs in human serum are 349 aM for miRNA-122, 374 aM for miRNA-223, and 311 aM for miRNA-21. High selectivity and accuracy of the SERS biosensor were proved by practical analysis in human serum. Moreover, the biosensor exhibited good practicability in multiplex detection of three miRNAs in 92 clinical sera from AFP-negative patients, patients before and after hepatectomy, recurred and relapse-free patients after hepatectomy, and hepatocellular carcinoma patients at distinct Barcelona clinic liver cancer stages. The experiment results demonstrate that our SERS-based assay is a promising candidate in clinical application and exhibited potential for the prediction, diagnosis, monitoring, and staging of cancers.

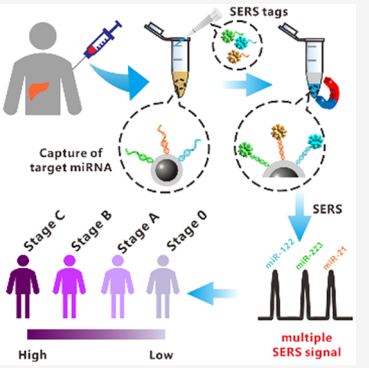

1. INTRODUCTION

Liver cancer is the fourth common malignancy that causes cancer-related deaths[1] and the second most lethal tumor worldwide.[2] Hepatocellular carcinoma (HCC) represents 85−90% of liver cancer.[3] It is well known that precise and early diagnosis and monitoring of HCC contribute to the prognosis of HCC and treatment effect. AFP (α-fetoprotein) has been widely accepted and utilized as an HCC biomarker. It is well known that 30−40% of HCC patients have a low abundance of AFP;[4−6] thus, it is of great significance to discriminate AFP-negative HCC (AFP levels <20 μg/L). Meanwhile, the monitoring of different stages of liver cancer is very important to enhance the therapeutic effect.

MicroRNA (miRNA), belonging to the group of small noncoding RNAs (usually 18−23 nucleotides), playing a key role in oncogenesis and tumor metastasis, has drawn significant attention as a novel biomarker for prediction, diagnosis, and monitoring treatment responses of cancer.[7,8] Many studies have identified the aberrant expression levels of multiple miRNAs in HCC compared to nontumor tissue.[9−13] Studies have been confirmed that certain miRNAs such as miR-122 and miR-223 are commonly repressed in HCC.[14−20] On the other hand, miR-21 is frequently overexpressed in HCC.[21−23] Xu et al. investigated the diagnostic effect of miR-122, miR-223, and miR-21 in HCC patients.[24] Other studies demonstrated that considerable miRNAs existed stably in human blood, which was the basis for the detection of miRNAs for diagnosis and prognosis of HCC.[25,26] Because of the low level of miRNA in body fluids, the development of new approaches for the ultrasensitive and multiple detections of HCC-related miRNAs is of great significance.[27]

Various miRNA detection technologies, such as traditional Northern blotting,[28] quantitative real-time PCR (qRT-PCR),[29] and microarrays,[30] are limited in clinical application because of their low sensitivity and inherent restriction in multiple detections, intricate steps, time consumption, and high cost. Recently, surface-enhanced Raman scattering (SERS) has emerged as a powerful technique for disease biomarker detection due to its high sensitivity and selectivity.[31−34]

Received: February 1, 2021
Accepted: May 13, 2021
Published: June 2, 2021

https://doi.org/10.1021/acs.analchem.1c00478
Anal. Chem. 2021, 93, 8799−8809

Besides, the unique narrow fingerprint SERS peaks for individual analytes are conducive to the simultaneous detection of multiple miRNAs.[35,36] Recently, some research groups have reported SERS-based miRNA detection methods.[37−41] However, simultaneous detection of several cancer-related miRNAs, especially in clinical practice, was rarely investigated. Therefore, the development of SERS probes with high specificity and sensitivity and SERS capture substrates with a reliable SERS signal and convenient synthesis process is imperative for sensitive and multiplex detection of miRNAs.

In recent years, experimental measurements[42−44] and theoretical calculations[45−47] have shown that the surface protrusions of complex Au nanostructures generate stronger enhancement of the electromagnetic field ("hot spots"). Meanwhile, more and more studies have led to the preparation of uniform gap-enhanced Raman tags (GERTs) for stable, controllable, and quantitative SERS enhancement, for example, gold nanobridged narrow intra-nanogap particles (Au-RNNPs).[48,49] DNA sequences can control the properties of metallic nanoparticles by mediating the inner and outer shape,[50−53] which holds great promise for designing diverse and multiplex SERS nanotags. However, the facile fabrication of uniform and well-defined GERTs to produce intense, stable, controllable, and differentiable SERS signals remains challenging.

Besides, Ag-coated magnetic nanoparticles (AgMNPs) consisted of a Fe_3O_4 core which greatly simplifies the separation step to improve reproducibility,[54,55] and an Ag shell provides an enhanced SERS signal. Nowadays, several methods have been developed to synthesize Ag-coated Fe_3O_4@SiO_2 microspheres,[56−58] but the Ag shell prepared by these methods is noncontinuous, which influences SERS ability and specific adsorption. Hence, mediating the thickness of the Ag shell by the facile fabrication process to produce intense SERS signals and maintain the magnetic separation ability of the magnetic NPs is crucial for synthesizing AgMNPs.

Herein, a multiplex sandwich SERS method was developed for the multiple and ultrasensitive detection of HCC-related miRNAs (miRNA-122, miRNA-21, and miRNA-223).[59] In this work, three DNA-engineered Raman dye-coded core−shell structure uniform stellate fractal gold nanoparticles (F-AuNPs) with stable, favorable, and multiple Raman signals were developed utilizing a controllable and convenient strategy. The density and amount of the Au surface protrusions that contribute greatly to the SERS signals were demonstrated by comparing the F-AuNPs with Au-RNNPs. Then, the F-AuNPs and AgMNPs were immobilized with three-probe DNA, and three capture DNAs specifically recognize three target miRNAs and form a sandwich hybridization complex. Moreover, the AgMNPs show great SERS properties and are used as excellent capturing substrates due to their outstanding magnetic response and low nonspecific adsorption. The limit of detection (LOD) of this multiplex assay was down to 311 aM for miRNA-21, 349 aM for miRNA-122, 374 aM for miRNA-223. The experiment results indicated that the proposed multiplex bioassay exhibited good selectivity, high sensitivity, and accuracy. Last but not least, the clinical potential of prediction, diagnosis, and monitoring of cancer patients utilizing our method was demonstrated by simultaneous detection of three HCC-related micro RNAs in 14 AFP-negative subjects, 11 patients before and after hepatectomy, 4 recurred after hepatectomy, 9 relapse-free patients, and 52 liver cancer patients with different Barcelona clinic liver cancer (BCLC) stages.

2. EXPERIMENTAL SECTION

2.1. Chemicals and Materials. Gold chloride trihydrate ($HAuCl_4·3H_2O$), ethylene imine polymer (PEI), silver nitrate ($AgNO_3$), 11-mercaptoundecanoic acid (MUA), 11-mercapto-1-undecanol (MU), *N*-(3-dimethylaminopropyl)-*N*′-ethylcarbodiimide hydrochloride (EDC), *N*-hydroxysuccinimide (NHS), polyethylene glycol (PEG, Mw = 10,000), and ammonia solution were purchased from Aladdin. Citric acid trisodium salt, rhodamine 6G (R6G), crystal violet (CV), 4-aminothiophenol (4-ATP), iron chloride hexahydrate ($FeCl_3·6H_2O$), ethylene glycol, and hydroxylammonium chloride ($NH_2OH·HCl$) were obtained from Macklin. Polyvinylpyrrolidone (PVP, Mw = 40,000) was obtained from Sigma-Aldrich. Sodium borohydride ($NaBH_4$) was purchased from Energy Chemical. The oligonucleotides (sequences are shown in Table S1) were purchased from Sangon Biotech. All ultrapure water was supplied by a Millipore water purification system (>18 MΩ cm resistivity, Millipore, USA).

2.2. Clinical Specimens. Human blood samples were obtained from HCC patients (n = 92) provided by Sun Yat-Sen University Cancer Center, and healthy volunteers (n = 2) were collected from the Guangdong Provincial Hospital of Traditional Chinese Medicine. Serum was obtained via venipuncture into vacutainer tubes and then centrifugation at 12,000 rpm (4 °C, 10 min). All specimens were stored at −80 °C until needed. Cancer diagnoses were confirmed by traditional examination at Sun Yat-sen University Cancer Center. Details of the clinical samples including the age, gender, AFP levels, PIVKA-II levels, and BCLC stages are provided in Tables S4−S7.

2.3. Synthesis of Fractal Gold Nanoparticle SERS Nanotags. *2.3.1. Preparation of PolyA30 and Raman Reporter-Modified AuNPs.* The gold nanoparticles (AuNPs) were prepared by referring to the previous method.[60] To prepare polyA30-modified AuNPs, first, thiolated polyA30 DNA (4 μL, 100 μM) was dispersed in Au seed colloid solution (100 μL). Next, sodium citrate-hydrochloric acid buffer (2 μL, 500 mM, pH = 3) was added. The mixture was incubated for 30 min before being centrifuged at 12,000 rpm for 15 min and then dispersed in 100 μL of phosphate-buffered saline (PBS) (0.1 M, pH = 7.4). For synthesis of Raman reporter-labeled polyA30-AuNPs, 30 μL of solution (10^{-1} M R6G, 10^{-2} M CV, and 10^{-2} M 4-ATP) was added to 300 μL of Poly30-AuNPs and incubated for 24 h (220 rpm, 25 °C). After removal of excess Raman dyes by centrifugation (12,000 rpm, 15 min), the Raman reporter-labeled DNA-AuNPs can be obtained.

2.3.2. Preparation of Fractal AuNPs. The fractal AuNPs were prepared according to the reported method with minor modification.[61] Briefly, 90 μL of PBS was added into 10 μL of polyA30-functionalized and Raman reporter-modified AuNPs; subsequently, PVP (50 μL, 1%), $NH_2OH·HCl$ (20 μL, 10 mM), and $HAuCl_4$ precursor (14 μL, 5 mM) were added successively under vigorous vortex. After incubation for 30 min, the mixture was centrifuged (6000 rpm, 10 min) and washed with PBS. By changing the volume of added $HAuCl_4$ (2, 8, 14, and 20 μL), four different morphologies of stellate gold nanoparticles with different SERS properties were obtained.

https://doi.org/10.1021/acs.analchem.1c00478
Anal. Chem. 2021, 93, 8799−8809

Scheme 1. Schematic Illustration of Multiplex miRNA Assay via the SERS Sandwich Strategy. R6G-, CV-, and 4-ATP-Encoded Fractal Au Nanoparticles were Utilized as SERS Tags, and Ag-Coated Magnetic Nanoparticles were Utilized as the Capture Substrate; (a) Schematic Processes of Synthesizing SERS tag; (b) Design and Synthesis of the Capture Substrate; (c) Detection Procedure of Multiple miRNAs Based on the Capture Substrate/miRNA/SERS Tag Sandwich Structure

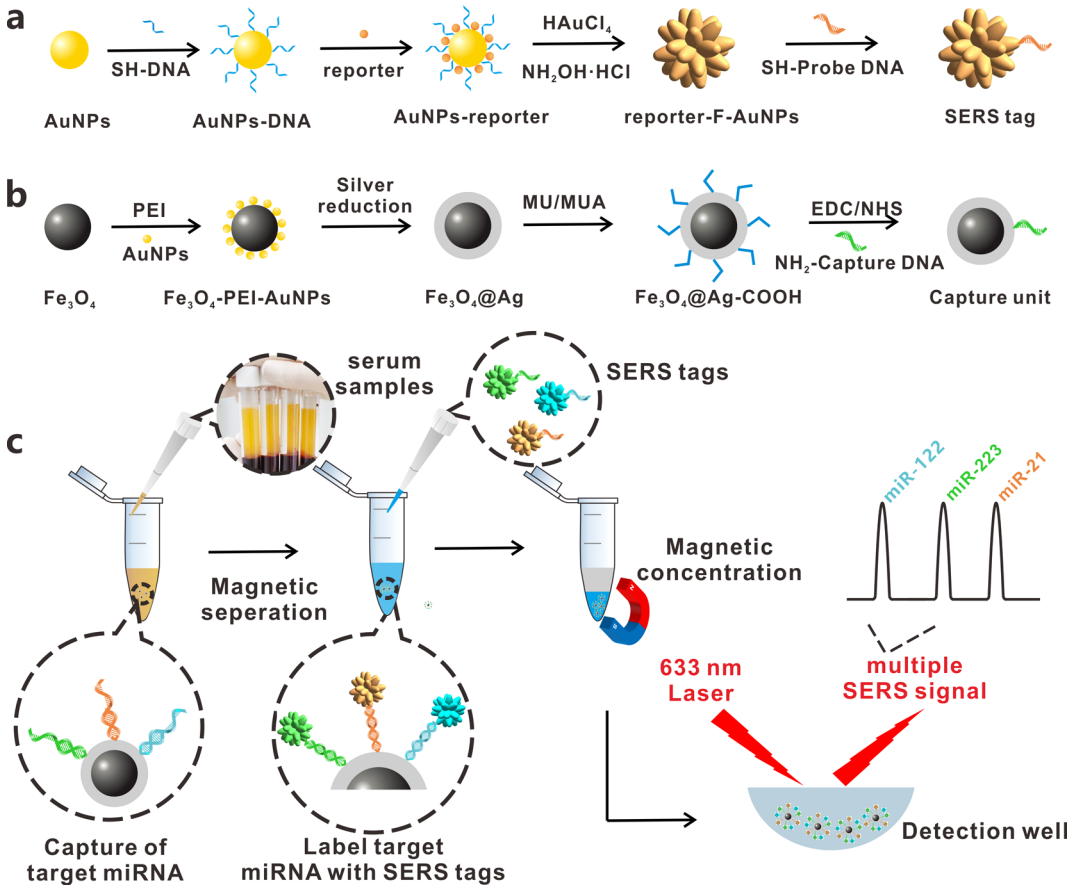

2.4. Synthesis of AgMNPs and Capture Substrates. *2.4.1. Synthesis of Fe_3O_4.* The Fe_3O_4 nanoparticles were prepared according to the reported method with minor modification.[62] In brief, 1.35 g of $FeCl_3{\cdot}6H_2O$ was dissolved in 40 mL of ethylene glycol followed by the addition of 1.0 g of polyethylene glycol and 3.6 g of $NaAc{\cdot}3H_2O$. After magnetic stirring for 24 h, the obtained solution was moved to a Teflon-lined stainless-steel autoclave, heating at 200 °C for 8 h. The black precipitate was collected and rinsed five times with ethanol and ultrapure water by magnetic separation. At last, the sediment was dried at 60 °C.

2.4.2. Synthesis of AgMNPs. The AgMNPs were synthesized following the previous method with some modification.[63] To assemble AuNPs on the surface of Fe_3O_4, PEI was utilized as a binding agent via electrostatic interaction. PEI (0.25 g) was added to 50 mL of ultrapure water; subsequently, 100 mg of the Fe_3O_4 NPs was added under sonication for 20 min. The resulting Fe_3O_4@PEI NPs were magnetically washed with ultrapure water five times. Au seed (4 nm) was synthesized by referring to the previous report with little modification.[64] Briefly, $HAuCl_4$ (10 mL, 5 mM) and TSC (10 mL, 5 mM) were added to 180 mL of ultrapure water. It was followed by adding $NaBH_4$ (5 mL, 0.1 M) and vigorously stirring at room temperature for 4 h to form an orange colloid solution. Finally, 120 mL of 4 nm AuNP solution was added to the above-prepared PEI-modified Fe_3O_4 NPs and sonicated for 1 h. The as-prepared Fe_3O_4@PEI-AuNP sediment was magnetically rinsed three times with water and ethanol and then dried at 60 °C.

To synthesize Ag-coated Fe_3O_4@PEI-AuNPs, different amounts of (2, 4, 6, 8, 10, 14, and 20 mg) $AgNO_3$ and PVP (300 mg) were added to ultrapure water (200 mL). After that, 10 mg of Fe_3O_4@PEI-AuNPs was added to the solution and mixed by sonication, followed by adding formaldehyde (150 μL) and ammonia (300 μL) under sonication for 5 min before being rinsed five times with ultrapure water.

3. RESULTS AND DISCUSSION

3.1. Design of SERS-Based Sandwich Immunoassay. As illustrated in Scheme 1a, three different Raman reporter molecule-encoded DNA-engineered SERS probes were modified with three-probe DNA (-SH complementary DNA to target miRNA-1, 2, and 3) to prepare SERS nanoprobes, respectively. Scheme 1b exhibits that the multiplexed capture substrate was formed by modifying three capture DNAs (-NH_2 complementary DNA-4, 5, and 6) on Ag-coated magnetic nanoparticles. The sandwich structure of capture substrate/miRNA/SERS tags was formed for the detection of three miRNAs, as illustrated in Scheme 1c. For the beginning, three capture DNA-functionalized AgMNPs were culture with a complex sample, containing the target miRNAs, irrelevant miRNAs, and other interferences. Subsequently, the target miRNA will specifically bind to capture DNA-modified AgMNPs due to the hybridization combination. The magnetic

https://doi.org/10.1021/acs.analchem.1c00478
Anal. Chem. 2021, 93, 8799−8809

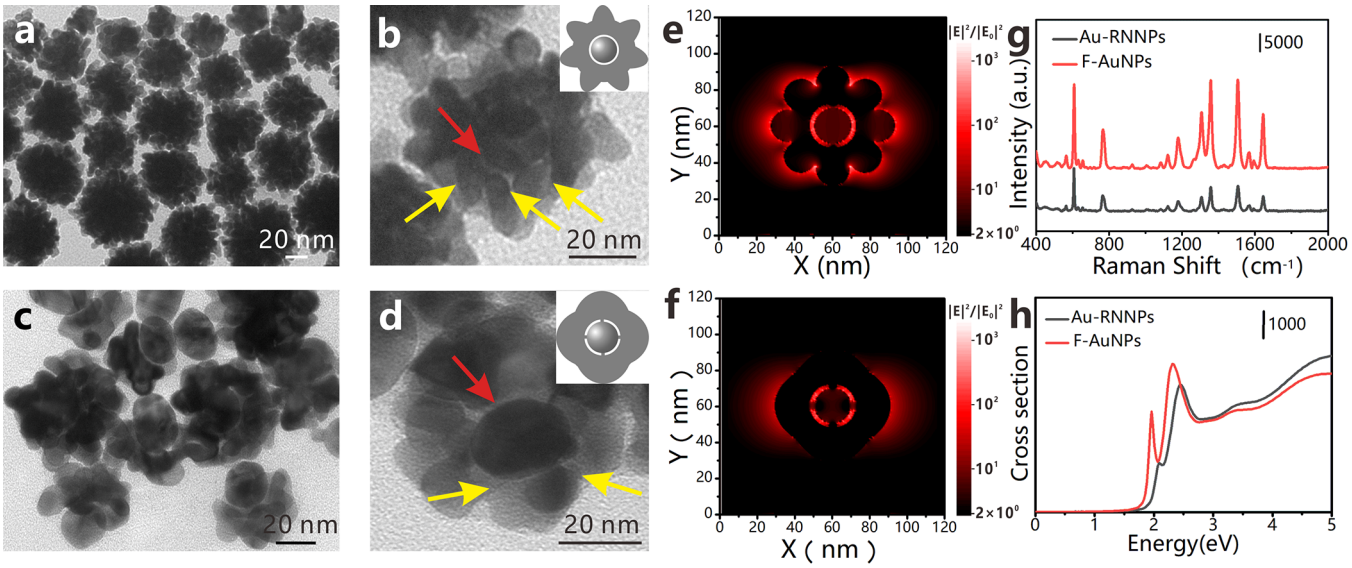

Figure 1. Comparison of fractal gold nanoparticles (F-AuNPs) and nanobridged nanogap particles (Au-RNNPs). Representative TEM images of F-AuNPs (a,b) and Au-RNNPs (c,d). The insets in panels (b,d) show the schematic diagrams of F-AuNPs and Au-RNNPs. FDTD-calculated electromagnetic field distribution of F-AuNPs (e) and Au-RNNPs (f). (g) SERS spectra of F-AuNPs (red) and Au-RNNPs (gray) that R6G utilized as the Raman reporter. The concentration of R6G was 5×10^{-3} M. (h) FDTD-simulated far-field absorption spectra of F-AuNPs (red) and Au-RNNPs (gray). SERS measurements were carried out by utilizing a 633 nm laser and 4 s acquisition time. The scale bar represents 20 nm.

nanoparticles contribute to the fast magnetic separation of the miRNA from the complex sample. Meanwhile, the magnetic concentration and Ag shell will greatly improve the SERS signal. Next, three-probe DNA-functionalized SERS tags modified with rhodamine 6G (R6G), crystal violet (CV), 4-aminothiophenol (4-ATP), respectively, corresponding to miRNA-122, miRNA-223, and miRNA-21 are added to form the sandwich structures. Finally, the SERS signal of the sandwich structures was detected after magnetic separation. In this strategy, R6G, CV, and 4-ATP were three Raman reporters and they can output distinctive Raman signals. Therefore, the proposed SERS sandwich assay can achieve the simultaneously sensitive and specific detection of multiple miRNAs.

3.2. Fabrication and Characterization of SERS Nanotags. Aiming to fabricate fractal gold nanoparticles, a seeded growth method was used. A poly30 adenine (A) DNA was anchored to the surface of 15 nm Au cores, and the core−shell structures can result when growing fractal outer shells on the DNA-coated AuNPs by reduction of $HAuCl_4$. TEM images confirm that F-AuNPs exhibited a typical size of 67 ± 3 nm (Figure 1a), while Au-RNNPs exhibited an overall diameter of 61 ± 3 nm (Figure 1c). Compared with the gold nanobridged nanogap particles (Au-RNNPs, using a thiolated 10-thymine (T10) DNA sequence to form a hollow gap), the gap size (~1 nm, red arrow in Figure 1b) of fractal gold nanoparticles (F-AuNPs) is narrower than that of the Au-RNNPs (3−4 nm, red arrow in Figure 1d). Studies have revealed that the trend of binding affinity between nucleic acid and gold nanoparticles is A > C ≥ G > T,[65,66] which can explain the abovementioned results. It is exhibited in the TEM images and schematic diagrams that both F-AuNPs and Au-RNNPs are core−shell structures, while plenty more nanogaps (1−3 nm, yellow arrows in Figure 1b) are presented on the rough surface of F-AuNPs. These external nanogaps greatly enhance the SERS intensity by forming electromagnetic hot spots. The electromagnetic field enhancement distributions of F-AuNPs and Au-RNNPs calculated by finite-difference time-domain (FDTD) are shown in Figure 1e,f, respectively. It can be seen that SERS hot spots on the external shell of F-AuNPs are much more than Au-RNNPs, and the calculation data indicated that the electromagnetic field enhancement of the inner gap of F-AuNPs is also stronger than that of Au-RNNPs. Figure 1g shows that the total Raman intensity of F-AuNPs (red) is roughly 1.5 times stronger than that of Au-RNNPs (gray) by comparing the Raman intensity at 615 cm^{-1} for R6G at a concentration of 5×10^{-3} M, while other conditions were held constant. Figure 1h exhibited the FDTD-simulated far-field absorption spectra of F-AuNPs (red) and Au-RNNPs (gray).

Figure S1a shows the TEM images of F-AuNPs during the growing process at different time points (0.5, 5, 10, 15, and 30 min) by terminating the reaction process. TEM images exhibited more nanoparticles and are presented in Figure S2. The STEM image of an individual F-AuNP in Figure S1b demonstrates the core−shell structure of the F-AuNPs. Figure S3 exhibits the TEM image of bare AuNPs. Figure S1c shows that with the modification DNA on the surface of AuNPs, a slight red shift is observed in UV−vis spectra of DNA-AuNPs (λ_{max} = 522 nm) and 4-ATP DNA-AuNPs (λ_{max} = 524 nm) compared with bare AuNPs (λ_{max} = 520 nm), indicating the successful assemble of DNA and 4-ATP molecules on the AuNPs. The resonance peak of F-AuNPs (λ_{max} = 628 nm) is red-shifted, indicating the strong plasmonic coupling of the protrusions on the F-AuNPs and the increase in the particle size (Figure S1d). We found that the morphology of the shell structure was dependent not only on the amount of precursor but also on the concentration of the Raman reporter. On the one hand, by varying the number of precursor $HAuCl_4$ (2, 8, 14, and 20 μL) while the other experimental factors were consistent, we tested the SERS performance of them and found that the optimized amount of $HAuCl_4$ is 14 μL (Figure S1f). The corresponding TEM images are shown in Figure S4. On the other hand, in a typical experiment of synthesis of 4-ATP-coded F-AuNPs, by controlling the concentration of 4-ATP (10^{-2}, 5×10^{-3}, 10^{-3}, 5×10^{-4}, 10^{-4}, and 10^{-5} M), we

https://doi.org/10.1021/acs.analchem.1c00478
Anal. Chem. 2021, 93, 8799−8809

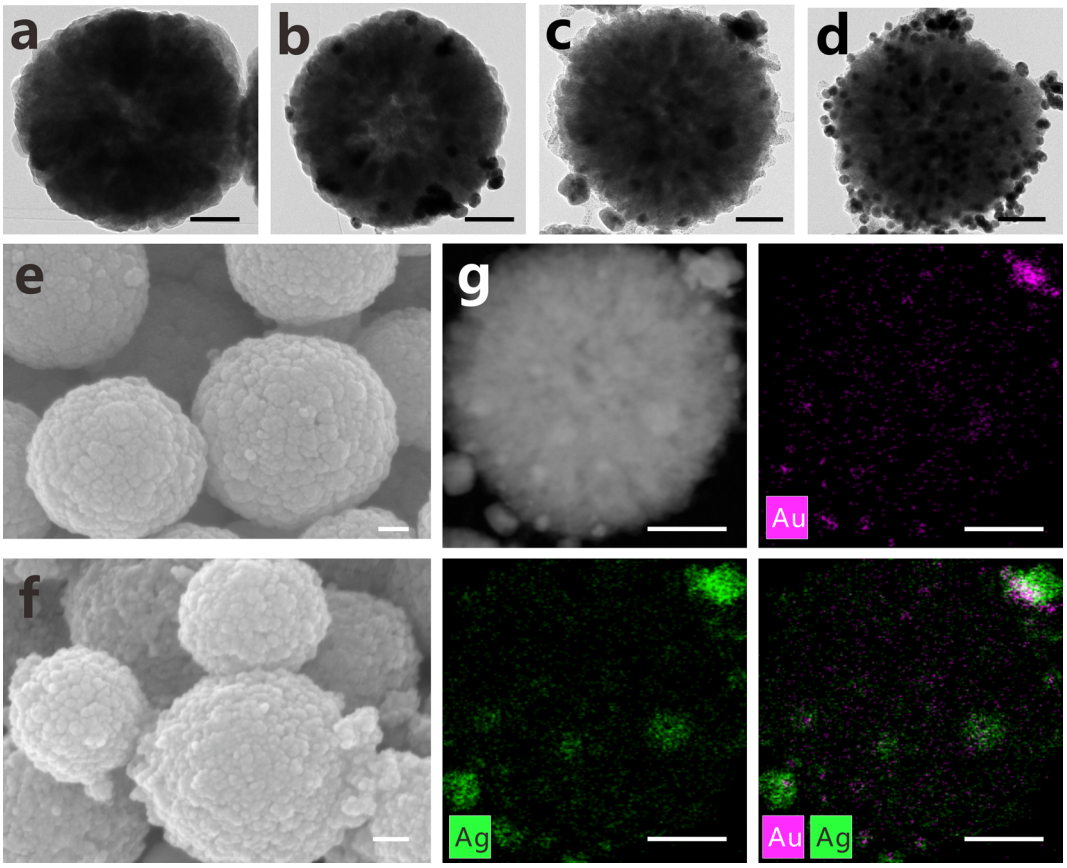

Figure 2. TEM images of (a) Fe_3O_4, (b) Fe_3O_4@PEI-AuNPs, (c) AgMNPs, and (d) sandwich complex structure of the SERS tags/miRNAs/capture substrate. SEM images of (e) Fe_3O_4 and (f) AgMNPs. (g) EDS mapping images of an individual AgMNP particle, purple represents Au and green represents Ag and overlapping of these two elements. The scale bars are 100 nm.

prepared a series of stellate nanostructures. TEM and SERS measurements exhibited morphology changes. The SERS intensity was the strongest at a 4-ATP concentration of 5×10^{-3} M (Figure S1g). The SERS spectra of the R6G-encoded F-AuNPs in 1% human serum demonstrated the reproducible SERS responses of nanoprobes in serum (Figure S1e), and the relative standard deviation (RSD) of the Raman intensity at 615 cm^{-1} is 3.7% (Figure S1h). Figure S5 shows the SERS spectra of three SERS nanoprobes, and the distinguishable spectra indicate that these nanoprobes can be applied to multiple analyses.

Based on these results, F-AuNPs synthesized with 14 μL of $HAuCl_4$, 5×10^{-3} M 4-ATP, CV, and R6G were chosen as SERS nanotags. The as-prepared F-AuNPs were further modified with probe DNA (-SH complementary DNA-1, 2, and 3) through the Au-S bond. A red shift can be observed in UV−vis spectra of DNA-F-AuNPs and F-AuNPs (Figure S6a). Zeta potential of DNA-F-AuNPs decreased compared with F-AuNPs, mostly owing to the functionalized negatively charged DNA on F-AuNPs, as shown in Figure S6b. All these results demonstrated the successful modification of DNA sequences on the F-AuNPs.

3.3. Fabrication and Characterization of the Magnetic Capture Substrate. To prepare Ag-coated Fe_3O_4@PEI-AuNPs, a seed-growth method was utilized. The obtained Fe_3O_4 NPs had a diameter of ~400 nm and their surfaces were rough, as shown in Figure 2a,e. Figure 2b illustrated that AuNPs were successfully absorbed on the outside of Fe_3O_4 NPs. It can also be proved by EDS and EDS mapping of Fe_3O_4 nanoparticles (Figure S7) and Fe_3O_4@PEI-AuNPs (Figure S8), in which the Au element existed uniformly. TEM images (Figure 2c) and SEM images (Figure 2f) confirm the successful assembly of Ag, indicating that the surface of AgMNPs becomes rougher than bare Fe_3O_4. In addition, EDS mapping of Ag-coated Fe_3O_4@PEI-AuNPs (Figure 2g) confirms the existence of Au and Ag, in which Au and Ag elements were uniformly present. Figure 2d shows that the sandwich structure of the SERS tags/miRNAs/capture substrate was successfully constructed, and a lot of spherical SERS tags were absorbed on the surface of AgMNPs through miRNA hybridization.

X-ray diffraction (XRD) images (Figure S9a) demonstrated the phase and purity of the as-prepared magnetic nanoparticles. The diffraction peaks of synthesized Fe_3O_4 (black curve) at 2θ values of 32.5, 35.7, 43.3, 53.7, 57.1, and 62.8 are corresponding to the (112), (211), (220), (024), (303), and (224) crystalline planes of the orthorhombic phase of Fe_3O_4 (JCPDS card no. 75-1609), respectively, which is consistent with the previous study.[60] A new XRD pattern of Fe_3O_4@PEI-AuNPs (red curve) at a 2θ value of 38.2 was shown, indicating the (111) crystalline plane of Au (PDF 04-0784, ICDD, 2004). The diffraction peak of AgMNPs (blue curve) at 2θ values of 38.1, 44.3, 64.4, 77.5, and 81.5 were indexed to the (111), (200), (220), and (311) crystalline planes of the Ag (PDF 04-0783, ICDD, 2004).[60] Figure S9b exhibited magnetic hysteresis loops of Fe_3O_4, Fe_3O_4@PEI-AuNPs, and AgMNPs. The magnetic saturation (MS) values of Fe_3O_4, Fe_3O_4@PEI-AuNPs, AgMNPs (8 mg $AgNO_3$), AgMNPs (14 mg $AgNO_3$),

https://doi.org/10.1021/acs.analchem.1c00478
Anal. Chem. 2021, 93, 8799−8809

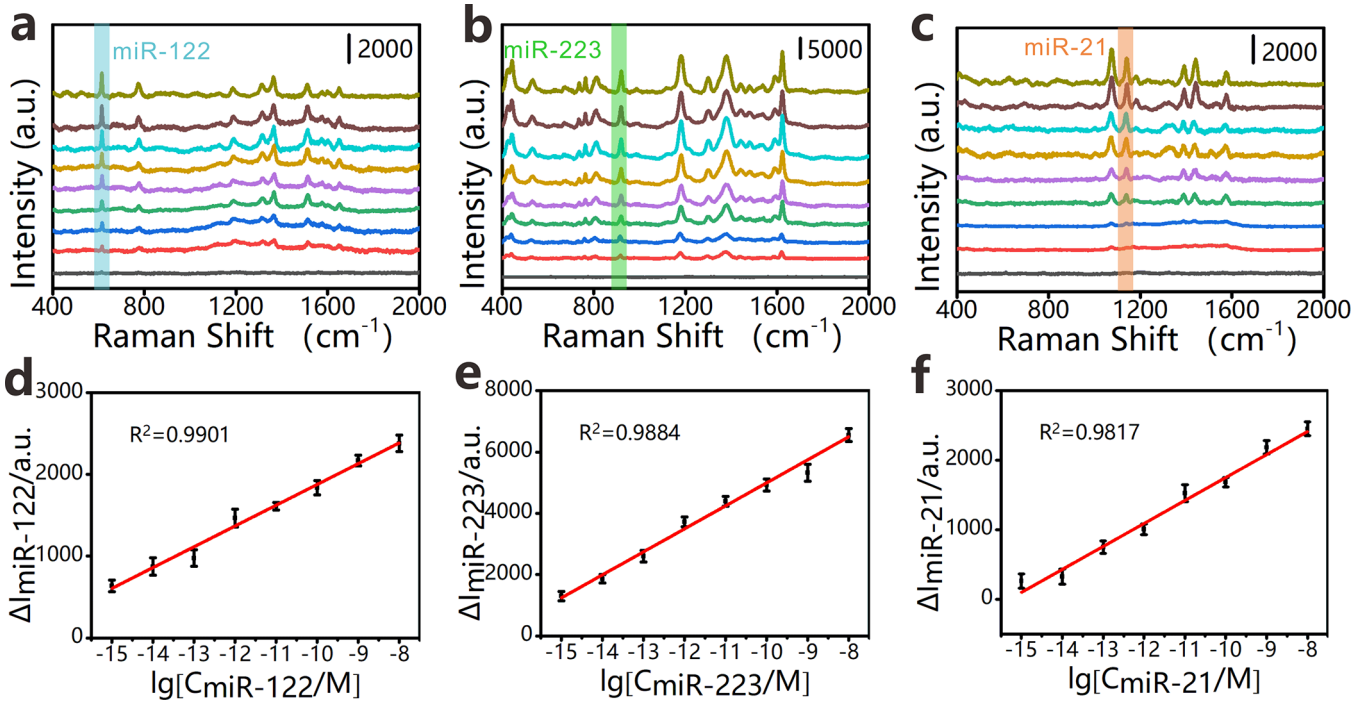

Figure 3. SERS spectra for various concentrations (blank, 1 fM, 10 fM, 100 fM, 1 pM, 10 pM, 100 pM, 1 nM, and 10 nM) of (a) miR-122, (b) miR-223, and (c) miR-21 in 1% human serum. Standard curves of the SERS peak intensity at 615, 918, and 1140 cm^{-1} against the concentrations of (d) miR-122, (e) miR-223, and (f) miR-21, respectively. The error bars stand for s. d. of triplicate measurements.

and AgMNPs (20 mg $AgNO_3$) are 81.0, 71.2, 59.7, 40.4, and 23.5 emu/g, respectively. The MS values of the magnetic nanoparticles were decreasing when functioned by AuNPs, PEI, and Ag. However, the synthesized AgMNPs still had the satisfying magnetic ability and can meet the demand for magnetic separation and enrichment.

Figure S9c shows the SERS responses of different thicknesses of Ag shell-coated AgMNPs using the characteristic Raman peaks of 4-ATP at 1040 cm^{-1}. The strongest SERS responsiveness was observed at the amount of 14 mg of $AgNO_3$ (the corresponding spectra are shown in Figure S10), and the SERS intensity decreased when the amount of $AgNO_3$ increased further. These data demonstrated that the integrity of the Ag shell of AgMNPs was conducive to improve the intensity of the SERS signal, which is consistent with the previous studies. However, when the Ag shell was too thick (20 mg $AgNO_3$), the SERS enhancement of AgMNPs was declined, and we presume that may be one of the reasons that the interaction between the Ag shell and Au core has become relatively hard to detect. Figure S9d shows the SERS spectrum of 500 μmol/L 4-ATP solution mixed with 2.5 mg/mL Fe_3O_4 NPs and AgMNPs (14 mg of $AgNO_3$). As shown in Figure S9e, the SERS signal of 2 months AgMNPs declined slightly but still produces a strong signal, indicating good stability of AgMNPs. The stability of the as-prepared AgMNPs was investigated by measuring the SERS performance of the freshly prepared AgMNPs and AgMNPs stored at 4 °C for 2 months by mixing with 10^{-6} M R6G. Figure S9f exhibits the SERS enhancement ability of the SERS probe (F-AuNPs) and capture substrate (AgMNPs). The Raman signal of F-AuNPs-R6G is 16 times stronger than that of AuNPs-R6G; moreover, SERS enhancement of AgMNPs is 12 times stronger than bare Fe_3O_4.

To prepare the capture substrate, AgMNPs were conjugated with capture DNA (-NH_2 complementary DNA-4, 5, and 6) using the EDC/NHS method. Briefly, the MUA and MU were added to form carboxylated AgMNPs, and EDC and NHS were utilized for forming an active ester that can copulate with amine-modified capture DNA. The UV−vis absorption spectrum of AgMNPs and DNA-AgMNPs shows no significant change (Figure S11a), and we assume that the larger overall size of the AgMNPs (~400 nm) than F-AuNPs (~67 nm) may be one of the reasons. The zeta potential of DNA-AgMNPs is lower than that of bare AgMNPs (Figure S11b), owing to the functionalization of negatively charged DNA on AgMNPs, indicating the successful loading of DNA on AgMNPs. The most suitable loading amount of capture DNA onto the AgMNPs was studied by a simple flocculation experiment using UV−vis spectroscopy. As shown in Figure S12, the optimal loading amount of capture DNA was 20 μM.

3.4. Detection of Single-Target miRNA. The sensitivity of detecting three HCC-related miRNAs using our SERS bioassay was investigated. It is well known that the high salt concentration and ionic strength in the serum may affect the stability of the F-AuNPs signal probe. When the serum was diluted 100 times with PBS buffer, the change in the UV−vis absorption peak of the F-AuNPs was negligible (Figure S13), so we used 1% serum for all of the following experiments. The stability of F-AuNP-jointed magnetic beads in 1% human serum was analyzed, as shown in Figure S14a, and the RSD of the Raman intensity at 615 cm^{-1} is 5.8% (Figure S14b), indicating the good stability of sandwich hybridization complexes. Figure 3a−c shows the concentration-dependent SERS spectra. It is shown that the SERS intensity increased corresponding to the increasing miRNA concentration, and the linear range is 1 fM to 10 nM. Figure 3d−f exhibits calibration curves of SERS intensity of Raman reporter molecules (615

https://doi.org/10.1021/acs.analchem.1c00478
Anal. Chem. 2021, 93, 8799−8809

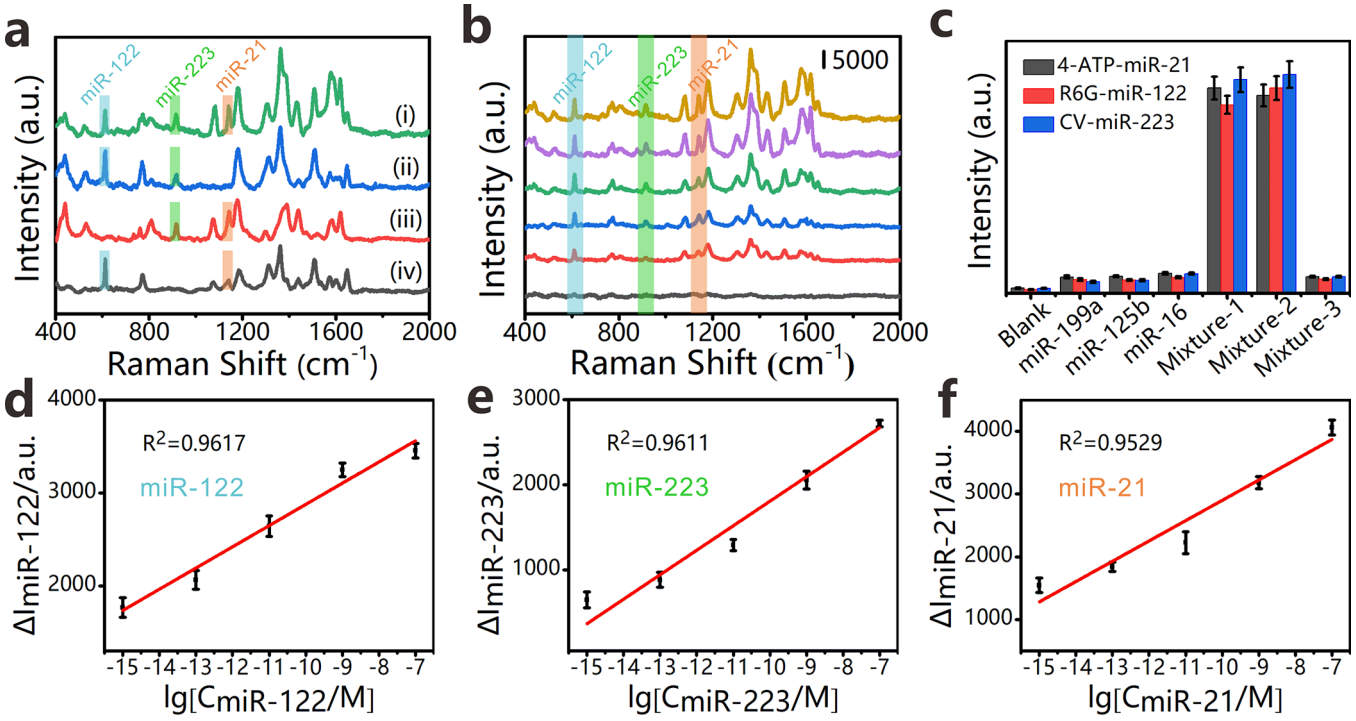

Figure 4. (a) Multiplex SERS spectra of miRNAs [(i) for miR-122, miR-223, and miR-21, (ii) for miR-122 and miR-223, (iii) for miR-223 and miR-21, and (iv) for miR-122 and miR-21]. (b) SERS spectra for triple-target miRNA detection (blank, 1 fM, 100 fM, 10 pM, 1 nM, and 100 nM). (c) Specificity evaluation of the proposed method for interfering miRNAs (miR-199a, miR-125b, and miR-16), mixture-1 (miR-122, miR-223, and miR-21), mixture-2 (miR-199a, miR-125b, miR-16, miR-122, miR-223, and miR-21), and mixture-3 (miR-122, miR-223, miR-21, and three corresponding antagomirs). Standard curves of the SERS peak intensity at 615, 918, and 1140 cm^{-1} against the concentrations of (d) miR-122, (e) miR-223, and (f) miR-21, respectively. The error bars stand for s. d. of triplicate measurements.

cm^{-1} for R6G, 918 cm^{-1} for CV, and 1140 cm^{-1} for 4-ATP), indicating a great linear relationship between the SERS signal and the logarithm of the miRNA concentration. The correlation coefficients (R^2) are 0.9901, 0.9884, and 0.9817 respectively.

To confirm the formation of sandwich complexes, detection of miR-21 using 4-ATP-modified F-AuNPs was performed. It is clearly shown in SEM images (Figure S15) and the SERS spectrum (Figure S16) that the nanoprobes were coupled with substrates through the hybridization with target miR-21, showing intense SERS signals, However, no binding of F-AuNPs was shown in the blank experiment, and no significant signal was observed. The incubation time of sandwich hybridization complexes was also studied (Figure S17). Moreover, the EDS mapping images (Figure S18) and EDS spectra (Figure S19) also demonstrated that the atoms % of the Au element of the F-AuNPs/miRNA/AgMNP sandwich structure was 6.03%, which was higher than that of bare AgMNPs (2.51%), indicating the hybridization of F-AuNPs on AgMNPs.

3.5. Multiplex Detection of Target miRNAs. The Raman spectra exhibited characteristics and separate peaks. As shown in Figure 4a, triple-target miRNA [(i) for miR-122, miR-223, and miR-21] and double-target miRNA [(ii) for miR-122 and miR-223, (iii) for miR-223 and miR-21, and (iv) for miR-122 and miR-21] detections were performed. The corresponding multiplexed characteristic Raman dye peaks were observed in the detection of double-target miRNAs and triple-target miRNAs. These experiments demonstrated that the SERS method exhibited good ability in multiple miRNA detection.

The sensitivity and selectivity of the simultaneous multiplex miRNA detection were assessed. Different concentrations of serial three miRNA samples (varied from 1 fM to 100 nM) were analyzed (Figure 4b). The simultaneous quantitative analysis of double-target miRNAs is shown in Figures S20–S22. Figure 4b exhibits the concentration-dependent SERS spectra. Figure 4d–f exhibits the calibration curves for the quantitative analysis of three miRNAs, and the correlation coefficients (R^2) are 0.9617, 0.9611, and 0.9529. Moreover, the LODs of simultaneous detection of miR-21, miR-122, and miR-223 were 311 aM, 349 aM, and 374 aM, respectively. These data confirm that this strategy for the detection of three miRNAs exhibited both a low LOD and a wide dynamic range.

Besides, we compared the detection results with other methods reported in other papers, including electrochemistry, colorimetric assay, fluorescence spectroscopy, SPR, lateral flow assay, and so forth, as shown in Table S2. The LOD of our method is lower than most of the multiple miRNA detection methods, showing the advantage and ability in the detection of ultralow concentration miRNA biomarkers in complex blood samples.

3.6. Specificity Assessment. To investigate the specificity of the simultaneous multiplex miRNA detection method, three noncomplementary miRNAs (miR-16, miR-199a, and miR-125b) and three specific antagomirs were utilized. Interfering noncomplementary miRNA solutions (100 pM) were added to the AgMNPs modified by three capture DNAs, respectively. After that three-probe DNA-encoded F-AuNPs were added to the solution. The experimental conditions were the same as the abovementioned conditions. As shown in Figure 4c, only weak signals could be detected in interfering miRNA groups and

https://doi.org/10.1021/acs.analchem.1c00478
Anal. Chem. 2021, 93, 8799−8809

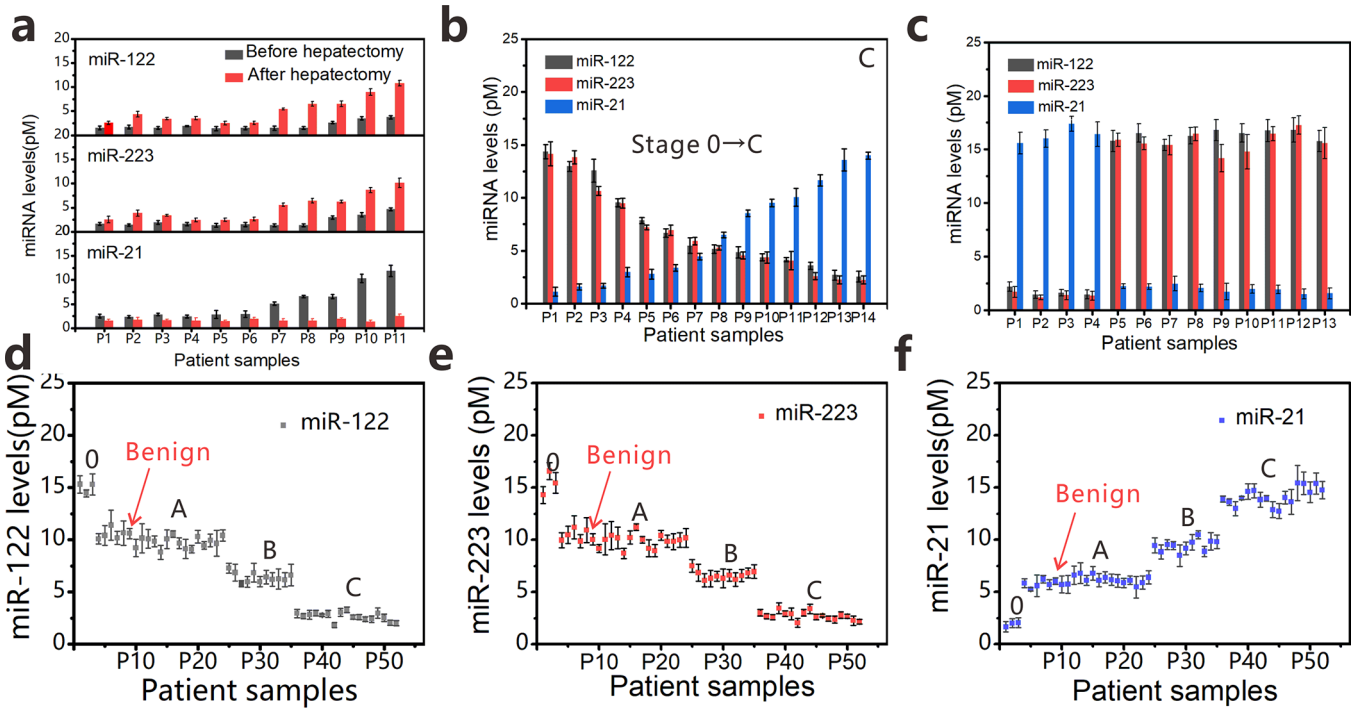

Figure 5. Sandwich assay of three miRNAs in serum specimens of HCC patients. (a) Levels of the three miRNAs before hepatectomy and 7 days after hepatectomy were measured by the sandwich assay. (b) Levels of the three miRNAs in the 14 AFP-negative clinical specimens. (c) Levels of three miRNAs relapsed within 1 year (P1−P4) and relapse-free after hepatectomy (P5−P13). The levels of (d) miR-21, (e) miR-122, and (f) miR-223 at different BCLC staging system stages (very early stage, early stage, intermediate stage, and advanced stage). The error bars stand for s. d. of triplicate measurements.

negligible signals showed in the blank group. Furthermore, by mixing noncomplementary miRNAs (100 pM) and target miRNAs (1 pM), the SERS signals obtained from mixture-2 (all six miRNAs) showed slight changes compared with the mixture-1 (three target miRNAs).

Furthermore, antagomirs, chemically modified antisense oligonucleotides complementary to specific miRNAs, have been shown to interfere with the miRNA function. Concerning this, three miRNA-specific antagomirs were designed and added contemporary with the target miRNAs, and all experimental conditions were the same as the abovementioned conditions. As shown in Figure 4c, compared with mixture-1, the SERS intensities of 615, 918, and 1140 cm^{-1} of mixture-3 were declined rapidly due to the influence of the antagomirs. These data indicate that this multiplex SERS assay exhibited excellent selectivity for target miRNAs.

3.7. Application in Human Serum Samples. To assess the reliability of our method, recoveries of different concentrations of miRNAs spiked in 1% healthy human serum were tested. As shown in Table S3, we assess the reliability of single miRNA and multiple miRNA detection, and recoveries we obtained are above 93%, indicating that the SERS biosensor exhibited good accuracy for miRNA detection in clinical applications.

3.8. Application in HCC Patients. To assess the performance of the proposed method in the prediction, diagnosis, and monitoring of HCC, we designed the following experiments. By simultaneous detection of the concentration of the miR-122, miR-223, and miR-21 of the same HCC patients (11 patients, Table S4), 1 day before hepatectomy and 7 days after hepatectomy, it is obvious that the level of miR-21 fell off after hepatectomy (Figure 5a), while the level of miR-122 and miR-223 increased after hepatectomy. Moreover, our assay was further applied in the detection of the AFP-negative patients (14 patients, Table S5, the clinical test results of AFP were all lower than 20 μg/L) and 52 HCC patients at different BCLC stages (Table S7 and Figure 5b,d−f), and the experimental results demonstrated that our method can successfully detect different levels of miRNAs in AFP-negative and different BCLC stage patients. The concentration of miR-21 increased with the stage of HCC patients, while the concentrations of miR-122 and miR-223 decreased, which means that this strategy has the potential ability to discriminate different stages of HCC patients. Meanwhile, by monitoring hepatectomy patients within 2 years, as shown in Figure 5c and Table S6, we found that the levels of the miR-21 of the patients who relapsed (P1−P4 in Figure 5c) within 1 year were higher than that of relapse-free patients (P5−P13 in Figure 5c); however, the level of miR-122 and miR-223 shows an opposite trend. The original data and details of these clinical samples including the age, gender, AFP levels, PIVKA-II levels, BCLC stages, and the three miRNA concentrations calculated according to the linear relationship between the Lg C_{miRNA} and SERS intensity are provided in Tables S4−S7. All the abovementioned results indicated that our SERS-based assay has a good potential application in the prediction, diagnosis, monitoring, and staging of HCC.

4. CONCLUSIONS

In summary, we developed Raman dye-modified fractal gold nanoparticles (F-AuNPs) as the SERS signal probe and Ag-coated magnetic nanoparticles (AgMNPs) as the capture substrate for simultaneous and ultrasensitive detection of three hepatocellular carcinoma-related micro RNAs (miR-122, miR-

https://doi.org/10.1021/acs.analchem.1c00478
Anal. Chem. 2021, 93, 8799−8809

223, and miR-21). By comparing to other thiolated DNA-mediated core−shell structure nanoparticles (Au-RNNPs), the fractal AuNP probe has a stronger and reproducible SERS performance. Also, the synthesized AgMNPs can achieve magnetic separation and exhibited favorable SERS activity, which contributes to further increase the sensitivity of the method. The good linear relationship between SERS intensity and the logarithm of the miRNA concentration was shown in the quantitative detection of miRNAs. The LOD of the quantitative detection reached the aM level. Multiplexed detection was also successfully applied in actual human serum samples and liver cancer patient serum assay, and the method exhibits excellent selectivity, specificity, and high accuracy under the interference of other miRNAs. Through the successful determination of target miRNAs in 14 AFP-negative patients, 13 patients before and after hepatectomy, 4 patients who relapsed (within 1 year) after hepatectomy, 9 relapse-free patients (2 years after hepatectomy), and 52 liver cancer patients with different BCLC stages (BCLC-0, BCLC-A, BCLC-B, and BCLC-C), the proposed SERS method opens new avenues for early diagnosis of cancer, the staging of HCC patients, and the prognosis of cancer and could offer a possibility for the rapid and ultrasensitive quantitative detection of other biomolecules.

■ ASSOCIATED CONTENT

Supporting Information

The Supporting Information is available free of charge at https://pubs.acs.org/doi/10.1021/acs.analchem.1c00478.

Experimental details, FDTD, characterization of F-AuNPs and AgMNPs, TEM, SERS spectra, UV−vis, zeta potential, EDS mapping images, optimization of capture DNA, stability analysis, SEM, multiplex SERS quantitative detection, sequences of oligonucleotides, comparison of the sensitivity of different methods, recovery results, and clinical background of the real samples (PDF)

■ AUTHOR INFORMATION

Corresponding Authors

Yun Zheng − *State Key Laboratory of Oncology in South China, Sun Yat-sen University Cancer Center, Guangzhou, Guangdong 510060, China*; Email: zhengyun@sysucc.org.cn

Zhengjin Jiang − *College of Pharmacy, Jinan University, Guangzhou, Guangdong 510632, China*; orcid.org/0000-0002-5612-4331; Email: jzjjackson@hotmail.com

Pinghua Sun − *College of Pharmacy, Jinan University, Guangzhou, Guangdong 510632, China*; Email: pinghuasunny@163.com

Haibo Zhou − *College of Pharmacy, Jinan University, Guangzhou, Guangdong 510632, China*; orcid.org/0000-0002-0098-5968; Email: haibo.zhou@jnu.edu.cn

Authors

Jiamin Wu − *College of Pharmacy, Jinan University, Guangzhou, Guangdong 510632, China*

Xia Zhou − *College of Pharmacy, Jinan University, Guangzhou, Guangdong 510632, China*

Ping Li − *College of Pharmacy, Jinan University, Guangzhou, Guangdong 510632, China*

Xiaoling Lin − *College of Pharmacy, Jinan University, Guangzhou, Guangdong 510632, China*

Jinhua Wang − *College of Pharmacy, Jinan University, Guangzhou, Guangdong 510632, China*

Ziwei Hu − *College of Pharmacy, Jinan University, Guangzhou, Guangdong 510632, China*

Pengcheng Zhang − *College of Chemistry and Chemical Engineering, Zhoukou Normal University, Zhoukou, Henan 466000, China*

Dong Chen − *State Key Laboratory of Oncology in South China, Sun Yat-sen University Cancer Center, Guangzhou, Guangdong 510060, China*

Huaihong Cai − *College of Chemistry and Materials Science, Jinan University, Guangzhou, Guangdong 510632, China*

Reinhard Niessner − *Institute of Hydrochemistry and Chair for Analytical Chemistry, Technical University of Munich, Munich D-81377, Germany*; orcid.org/0000-0002-3781-0248

Christoph Haisch − *Institute of Hydrochemistry and Chair for Analytical Chemistry, Technical University of Munich, Munich D-81377, Germany*; orcid.org/0000-0002-6344-6750

Complete contact information is available at: https://pubs.acs.org/10.1021/acs.analchem.1c00478

Author Contributions

J.W. and X.Z. are cofirst authors and contributed equally to this work. J.W., H.Z., Z.J., and Z.H. conceived and designed the experiments. J.W., X.Z., J.W., X.L., and P.L. performed the experiments. P.Z. contributed to the simulated calculations. D.C. and Y.Z. provided the clinical specimens of liver cancer patients. J.W., P.S., H.C., R.N., C.H., and H.Z. wrote and revised the paper. All authors discussed the results and commented on the manuscript.

Notes

The authors declare no competing financial interest.

■ ACKNOWLEDGMENTS

This work was supported by the National Natural Science Foundation of China (81773684, 81872759, and 82003707), Guangdong Natural Science Funds for Distinguished Young Scholars (2018B030306033), Science and Technology Program of Guangzhou (202102010097), Pearl River Talent Program (2017GC010363), Basic and Applied Basic Research Foundation of Guangdong Province (2020A1515110436), and the 67th Batch of China Postdoctoral Science Foundation (2020M673087).

■ REFERENCES

(1) Villanueva, A. *N. Engl. J. Med.* **2019**, *380*, 1450−1462.

(2) Jemal, A.; Ward, E. M.; Johnson, C. J.; Cronin, K. A.; Ma, J. M.; Ryerson, A. B.; Mariotto, A.; Lake, A. J.; Wilson, R.; Sherman, R. L.; Anderson, R. N.; Henley, S. J.; Kohler, B. A.; Penberthy, L.; Feuer, E. J.; Weir, H. K. *J. Natl. Cancer Inst.* **2017**, *109*, djx030.

(3) European Association for the Study of the Liver. *J. Hepatol.* **2018**, *69*, 182−236.

(4) Forner, A.; Bruix, J. *Lancet Oncol.* **2012**, *13*, 750−751.

(5) Toso, C.; Asthana, S.; Bigam, D. L.; Shapiro, A. M. J.; Kneteman, N. M. *Hepatology* **2009**, *49*, 832−838.

(6) Ye, X.; Li, C.; Zu, X.; Lin, M.; Liu, Q.; Liu, J.; Xu, G.; Chen, Z.; Xu, Y.; Liu, L.; Luo, D.; Cao, Z.; Shi, G.; Feng, Z.; Deng, H.; Liao, Q.; Cai, C.; Liao, D.; Wang, J.; Jin, J.; et al. *Hepatology* **2019**, *69*, 2489−2501.

(7) Lewis, B. P.; Burge, C. B.; Bartel, D. P. *Cell* **2005**, *120*, 15−20.
(8) Lu, J.; Getz, G.; Miska, E. A.; Alvarez-Saavedra, E.; Lamb, J.; Peck, D.; Sweet-Cordero, A.; Ebert, B. L.; Mak, R. H.; Ferrando, A. A.; Downing, J. R.; Jacks, T.; Horvitz, H. R.; Golub, T. R. *Nature* **2005**, *435*, 834−838.
(9) Kutay, H.; Bai, S.; Datta, J.; Motiwala, T.; Pogribny, I.; Frankel, W.; Jacob, S. T.; Ghoshal, K. *J. Cell. Biochem.* **2006**, *99*, 671−678.
(10) Bai, X.; Liu, Z.; Shao, X.; Wang, D.; Dong, E.; Wang, Y.; Wu, C.; Yuan, Y.; Lu, X.; Li, C. *PLoS One* **2019**, *14*, No. e0211581.
(11) Li, L.-M.; Hu, Z.-B.; Zhou, Z.-X.; Chen, X.; Liu, F.-Y.; Zhang, J.-F.; Shen, H.-B.; Zhang, C.-Y.; Zen, K. *Cancer Res.* **2010**, *70*, 9798−9807.
(12) Meng, F.; Henson, R.; Wehbe−Janek, H.; Ghoshal, K.; Jacob, S. T.; Patel, T. *Gastroenterology* **2007**, *133*, 647−658.
(13) Tsai, W.-C.; Hsu, P. W.-C.; Lai, T.-C.; Chau, G.-Y.; Lin, C.-W.; Chen, C.-M.; Lin, C.-D.; Liao, Y.-L.; Wang, J.-L.; Chau, Y.-P.; Hsu, M.-T.; Hsiao, M.; Huang, H.-D.; Tsou, A.-P. *Hepatology* **2009**, *49*, 1571−1582.
(14) Chang, J.; Nicolas, E.; Marks, D.; Sander, C.; Lerro, A.; Buendia, M. A.; Xu, C.; Mason, W. S.; Moloshok, T.; Bort, R.; Zaret, K. S.; Taylor, J. M. *RNA Biol.* **2004**, *1*, 106−113.
(15) Dong, Y. W.; Wang, R.; Cai, Q. Q.; Qi, B.; Wu, W.; Zhang, Y. H.; Wu, X. Z. *J. Hepatol.* **2014**, *60*, 792−801.
(16) Ji, J.; Zheng, X.; Forgues, M.; Yamashita, T.; Wauthier, E. L.; Reid, L. M.; Wen, X.; Song, Y.; Wei, J. S.; Khan, J.; Thorgeirsson, S. S.; Wang, X. W. *Hepatology* **2015**, *62*, 829−840.
(17) Jiang, J.; Gusev, Y.; Aderca, I.; Mettler, T. A.; Nagorney, D. M.; Brackett, D. J.; Roberts, L. R.; Schmittgen, T. D. *Clin. Cancer Res.* **2008**, *14*, 419−427.
(18) Murakami, Y.; Yasuda, T.; Saigo, K.; Urashima, T.; Toyoda, H.; Okanoue, T.; Shimotohno, K. *Oncogene* **2006**, *25*, 2537−2545.
(19) Wong, Q. W. L.; Lung, R. W. M.; Law, P. T. Y.; Lai, P. B. S.; Chan, K. Y. Y.; To, K. F.; Wong, N. *Gastroenterology* **2008**, *135*, 257−269.
(20) Zhou, J.; Yu, L.; Gao, X.; Hu, J.; Wang, J.; Dai, Z.; Wang, J.-F.; Zhang, Z.; Lu, S.; Huang, X.; Wang, Z.; Qiu, S.; Wang, X.; Yang, G.; Sun, H.; Tang, Z.; Wu, Y.; Zhu, H.; Fan, J. *J. Clin. Oncol.* **2011**, *29*, 4781−4788.
(21) Jemal, A.; et al. *Ca-Cancer J. Clin.* **2011**, *61*, 69.
(22) Ladeiro, Y.; Couchy, G.; Balabaud, C.; Bioulac-Sage, P.; Pelletier, L.; Rebouissou, S.; Zucman-Rossi, J. *J. Hepatol.* **2008**, *47*, 1955−1963.
(23) Meng, F.; Henson, R.; Wehbe−Janek, H.; Ghoshal, K.; Jacob, S. T.; Patel, T. *Gastroenterology* **2007**, *133*, 647−658.
(24) Xu, J.; Wu, C.; Che, X.; Wang, L.; Yu, D.; Zhang, T.; Huang, L.; Li, H.; Tan, W.; Wang, C.; Lin, D. *Mol. Carcinog.* **2011**, *50*, 136−142.
(25) Chen, X.; Ba, Y.; Ma, L.; Cai, X.; Yin, Y.; Wang, K.; Guo, J.; Zhang, Y.; Chen, J.; Guo, X.; Li, Q.; Li, X.; Wang, W.; Zhang, Y.; Wang, J.; Jiang, X.; Xiang, Y.; Xu, C.; Zheng, P.; Zhang, J.; et al. *Cell Res.* **2008**, *18*, 997−1006.
(26) Mitchell, P. S.; Parkin, R. K.; Kroh, E. M.; Fritz, B. R.; Wyman, S. K.; Pogosova-Agadjanyan, E. L.; Peterson, A.; Noteboom, J.; O'Briant, K. C.; Allen, A.; Lin, D. W.; Urban, N.; Drescher, C. W.; Knudsen, B. S.; Stirewalt, D. L.; Gentleman, R.; Vessella, R. L.; Nelson, P. S.; Martin, D. B.; Tewari, M. *Proc. Natl. Acad. Sci. U.S.A.* **2008**, *105*, 10513−10518.
(27) Lin, S.; Gregory, R. I. *Nat. Rev. Cancer* **2015**, *15*, 321−333.
(28) Lee, R. C.; Ambros, V. *Science* **2001**, *294*, 862−864.
(29) Thomou, T.; Mori, M. A.; Dreyfuss, J. M.; Konishi, M.; Sakaguchi, M.; Wolfrum, C.; Rao, T. N.; Winnay, J. N.; Garcia-Martin, R.; Grinspoon, S. K.; Gorden, P.; Kahn, C. R. *Nature* **2017**, *545*, 252.
(30) Li, Q.; Lowey, B.; Sodroski, C.; Krishnamurthy, S.; Alao, H.; Cha, H.; Chiu, S.; El-Diwany, R.; Ghany, M. G.; Liang, T. J. *Nat. Commun.* **2017**, *8*, 1789.
(31) Nie, S.; Emory, S. R. *Abstr. Pap. Am. Chem. Soc.* **1997**, *275*, 1102−1106.
(32) Shachaf, C.; Elchuri, S.; Zhu, J.; Nguyen, L.; Zhang, J. W.; Sun, L.; Chang, S.; Nolan, G. *Cancer Res.* **2008**, *68*, 4742.
(33) Zhou, X.; Hu, Z.; Yang, D.; Xie, S.; Jiang, Z.; Niessner, R.; Haisch, C.; Zhou, H.; Sun, P. *Adv. Sci.* **2020**, *7*, 2001739.
(34) Yuan, K.; Mei, Q.; Guo, X.; Xu, Y.; Yang, D.; Sánchez, B. J.; Sheng, B.; Liu, C.; Hu, Z.; Yu, G.; Ma, H.; Gao, H.; Haisch, C.; Niessner, R.; Jiang, Z.; Zhou, H. *Chem. Sci.* **2018**, *9*, 8781−8795.
(35) Porter, M. D.; Lipert, R. J.; Siperko, L. M.; Wang, G.; Narayanan, R. *Chem. Soc. Rev.* **2008**, *37*, 1001−1011.
(36) Mulvaney, S. P.; Musick, M. D.; Keating, C. D.; Natan, M. J. *Langmuir* **2003**, *19*, 4784−4790.
(37) Liu, C.; Chen, C.; Li, S.; Dong, H.; Dai, W.; Xu, T.; Liu, Y.; Yang, F.; Zhang, X. *Anal. Chem.* **2018**, *90*, 10591−10599.
(38) Liu, J.; Wen, Y.; He, H.; Chen, H.-Y.; Liu, Z. *Chem. Sci.* **2018**, *9*, 7241−7246.
(39) Meng, X.; Wang, H.; Yang, M.; Li, J.; Yang, F.; Zhang, K.; Dong, H.; Zhang, X. *Anal. Chem.* **2021**, *93*, 1693−1701.
(40) Meng, X.; Zhang, K.; Yang, F.; Dai, W.; Lu, H.; Dong, H.; Zhang, X. *Anal. Chem.* **2020**, *92*, 8333−8339.
(41) Tang, S.; Gu, Y.; Lu, H.; Dong, H.; Zhang, K.; Dai, W.; Meng, X.; Yang, F.; Zhang, X. *Anal. Chim. Acta* **2018**, *1004*, 1−9.
(42) Jia, W.; Li, J.; Jiang, L. *ACS Appl. Mater. Interfaces* **2013**, *5*, 6886−6892.
(43) Rodríguez-Lorenzo, L.; Álvarez-Puebla, R. A.; de Abajo, F. J. G.; Liz-Marzán, L. M. J. *J. Phys. Chem. C* **2010**, *114*, 7336−7340.
(44) You, H.; Ji, Y.; Wang, L.; Yang, S.; Yang, Z.; Fang, J.; Song, X.; Ding, B. *J. Mater. Chem.* **2012**, *22*, 1998−2006.
(45) Bakr, O. M.; Wunsch, B. H.; Stellacci, F. *Chem. Mater.* **2006**, *18*, 3297−3301.
(46) Hao, E.; Bailey, R. C.; Schatz, G. C.; Hupp, J. T.; Li, S. *Nano Lett.* **2004**, *4*, 327−330.
(47) Kumar, P. S.; Pastoriza-Santos, I.; Rodriguez-Gonzalez, B.; Garcia de Abajo, F. J.; Liz-MarzanPastoriza-Santos, L. M. I.; Rodriguez-Gonzalez, B.; Garcia de Abajo, F. J.; Liz-Marzan, L. M. *Nanotechnology* **2008**, *19*, 015606.
(48) Kang, J. W.; So, P. T. C.; Dasari, R. R.; Lim, D.-K.; Lim, D. K. *Nano Lett.* **2015**, *15*, 1766−1772.
(49) Lim, D.-K.; Jeon, K.-S.; Hwang, J.-H.; Kim, H.; Kwon, S.; Suh, Y. D.; Nam, J.-M. *Nat. Nanotechnol.* **2011**, *6*, 452−460.
(50) Shen, J.; Xu, L.; Wang, C.; Pei, H.; Tai, R.; Song, S.; Huang, Q.; Fan, C.; Chen, G. *Angew. Chem., Int. Ed.* **2014**, *53*, 8338−8342.
(51) Tan, L. H.; Yue, Y.; Satyavolu, N. S. R.; Ali, A. S.; Wang, Z.; Wu, Y.; Lu, Y. *J. Am. Chem. Soc.* **2015**, *137*, 14456−14464.
(52) Wang, Z.; Zhang, J.; Ekman, J. M.; Kenis, P. J. A.; Lu, Y. *Nano Lett.* **2010**, *10*, 1886−1891.
(53) Wu, J.; Tan, L. H.; Hwang, K.; Xing, H.; Wu, P.; Li, W.; Lu, Y. *J. Am. Chem. Soc.* **2014**, *136*, 15195−15202.
(54) Donnelly, T.; Smith, W. E.; Faulds, K.; Graham, D. *Chem. Commun.* **2014**, *50*, 12907−12910.
(55) Mahmoudi, M.; Serpooshan, V. *ACS Nano* **2012**, *6*, 2656−2664.
(56) Esmaeili, N.; Pirbazari, A. E.; Khodaee, Z. *Water Treat.* **2018**, *114*, 251−264.
(57) Han, B.; Choi, N.; Kim, K. H.; Lim, D. W.; Choo, J. *J. Phys. Chem. C* **2011**, *115*, 6290−6296.
(58) Yang, L.; Bao, Z.; Wu, Y.; Liu, J. *Raman Spectrosc.* **2012**, *43*, 848−856.
(59) Roberts, L. R. *N. Engl. J. Med.* **2008**, *359*, 420−422.
(60) Hu, Z.; Xie, M.; Yang, D.; Chen, D.; Jian, J.; Li, H.; Yuan, K.; Jiang, Z.; Zhou, H. *RSC Adv.* **2017**, *7*, 34746−34754.
(61) Shen, J.; Liang, L.; Xiao, M.; Xie, X.; Wang, F.; Li, Q.; Ge, Z.; Li, J.; Shi, J.; Wang, L.; Li, L.; Pei, H.; Fan, C. *J. Am. Chem. Soc.* **2019**, *141*, 11938−11946.
(62) Hu, H.; Wang, Z.; Pan, L.; Zhao, S.; Zhu, S. *J. Phys. Chem. C* **2010**, *114*, 7738−7742.
(63) Wang, J.; Wu, X.; Wang, C.; Shao, N.; Dong, P.; Xiao, R.; Wang, S. *ACS Appl. Mater. Interfaces* **2015**, *7*, 20919−20929.
(64) Wang, C.; Wang, C.; Wang, X.; Wang, K.; Zhu, Y.; Rong, Z.; Wang, W.; Xiao, R.; Wang, S. *ACS Appl. Mater. Interfaces* **2019**, *11*, 19495−19505.

https://doi.org/10.1021/acs.analchem.1c00478
Anal. Chem. 2021, 93, 8799−8809

(65) Koo, K. M.; Carrascosa, L. G.; Shiddiky, M. J. A.; Trau, M. *Anal. Chem.* **2016**, *88*, 6781−6788.
(66) Peng, L.; Zhang, P.; Chai, Y.; Yuan, R. *Anal. Chem.* **2017**, *89*, 5036−5042.

https://doi.org/10.1021/acs.analchem.1c00478
Anal. Chem. 2021, 93, 8799−8809